

Convergence of splitting methods on rotating grids for the magnetized Vlasov equation

Nils Schild¹, Mario R ath¹, Klaus Hallatschek¹, and Katharina Kormann²

¹*Max Planck Institut for Plasma Physics, Germany*

²*Ruhr University Bochum, Germany*

Abstract

Semi-Lagrangian solvers for the Vlasov system offer noiseless solutions compared to Lagrangian particle methods and can handle larger time steps compared to Eulerian methods. In order to reduce the computational complexity of the interpolation steps, it is common to use a directional splitting. However, this typically yields the wrong angular velocity. In this paper, we analyze a semi-Lagrangian method that treats the $\mathbf{v} \times \mathbf{B}$ term with a rotational grid and combines this with a directional splitting for the remaining terms. We analyze the convergence properties of the scheme both analytically and numerically. The favorable numerical properties of the rotating grid solution are demonstrated for the case of ion Bernstein waves.

1 Introduction and Problem Description

A kinetic description of (collisionless) plasmas evolves the phase-space distribution function f_s of particles of species s (of charge q_s and mass m_s in external and self-consistent electromagnetic fields \mathbf{E} and \mathbf{B} by the so-called Vlasov equation

$$\partial_t f_s(\mathbf{x}, \mathbf{v}, t) + \mathbf{v} \cdot \nabla_{\mathbf{x}} f_s(\mathbf{x}, \mathbf{v}, t) + \frac{q_s}{m_s} (\mathbf{E}(\mathbf{x}, t) + \mathbf{v} \times \mathbf{B}) \cdot \nabla_{\mathbf{v}} f_s(\mathbf{x}, \mathbf{v}, t) = 0. \quad (1)$$

While this hyperbolic conservation law appears linear for given electromagnetic fields, the equation is non-linearly coupled to Maxwell's equations for self-consistent fields. In this paper, we consider a simplified model where the self-consistent magnetic field is neglected, and the background magnetic field \mathbf{B}_0 is considered to be a constant field in both time and space-aligned with the \hat{e}_z axis. Our physical use cases are motivated by ion transport properties in plasmas. Those can be described by assuming adiabatic electrons, which handles the electron movement implicitly and a quasi-neutrality assumption. We normalize physical quantities ($q = m = T = 1$) such that the ion motion in our model is described by

$$\partial_t f(\mathbf{x}, \mathbf{v}, t) + \mathbf{v} \cdot \nabla_{\mathbf{x}} f(\mathbf{x}, \mathbf{v}, t) + (\mathbf{E}(\mathbf{x}, t) + \mathbf{v} \times \mathbf{B}_0) \cdot \nabla_{\mathbf{v}} f(\mathbf{x}, \mathbf{v}, t) = 0 \quad (2)$$

$$\phi(\mathbf{x}, t) = n(\mathbf{x}, t) = \int f(\mathbf{x}, \mathbf{v}, t) d\mathbf{v}, \quad \mathbf{E}(\mathbf{x}, t) = -\nabla_{\mathbf{x}} \phi(\mathbf{x}, t). \quad (3)$$

and was used to investigate the limits of gyrokinetics [17] and study turbulence phenomena that are not covered by gyrokinetic models [16]. The authors emphasize that the introduced rotating grid is not limited to this model but can be utilized for any electrostatic model with a constant magnetic background field. An example would be the Vlasov Poisson model is widely used to verify numerical methods.

The backward semi-Lagrangian method discretizes the distribution function on a grid. The point-wise solution at a given grid point is propagated forward in time in two steps: First, the characteristic equations of motion associated with the hyperbolic conservation properties of eq. (2) are solved backward in time until the previous time step. Then, the solution at the grid point at the new time step is given by the solution at the previous time step at this foot of the characteristic curve. In order to simplify the solution of the characteristic, it is common to use a directional splitting that solves the characteristics along one dimension at a time and then combines the six steps in Lie, Strang, or higher-order splitting method (cf. [6]). Due to the splitting, the characteristic equations are not solved exactly and, in particular an inexact solution of the rotation induced by the term $\mathbf{v} \times \mathbf{B}$ can yield a numerical heating of the plasma as explained in [19]. Therefore, several approaches have been proposed in the literature to better approximate in particular that rotation induced by the $\mathbf{v} \times \mathbf{B}$ term.

This paper starts with the idea of a rotating grid, as proposed by Kornmann, Reuter & Rampp [12] which removes the rotation induced by $\mathbf{v} \times \mathbf{B}$

from the advection step by pushing it into a coordinate transform of the computational grid. We extend the previous work by the transformation of the full Vlasov equation into the computational domain. Additionally, we provide a convergence analysis for splitting methods on the rotating grid.

The rotating grid has two main advantages compared to the direct solution of eq. (2). Firstly, the rotation removes the \mathbf{v} dependence of the \mathbf{v} -advective part of the Vlasov equation. The remaining \mathbf{v} advection can be split less expensively without loss of accuracy as will be explained in section 3 on splitting methods. Secondly, the rotating grid gives more accurate results compared to the splitting schemes applied to eq. (2) with the $\mathbf{v} \times \mathbf{B}$ term as is shown in section 4. In certain situations with strong background fields, the rotational grid can also lead to more local interpolation stencils, which is of interest in a distributed solution.

Alternative approaches to accurately solve the rotational motion have been proposed in the literature. Schmitz & Grauer [19] proposed a backsubstitution method applied to the Boris scheme. Bernier, Casas & Crouseilles [1] propose to decompose a two-dimensional rotational motion into a product of three shear transformations that amount to one-dimensional advection steps each. Compared to the latter approach, the use of a rotational grid has the advantage that the number of split steps is smaller, which significantly reduces the computational cost to calculate the solution.

The main goal of this paper is to provide a complete analysis of the convergence properties of the semi-Lagrangian method with a rotational grid and a directional splitting. Convergence of semi-Lagrangian schemes has been studied in [2] for the one-dimensional Vlasov–Poisson system and by Einkemmer & Ostermann [8] with a particular focus on the directional splitting time accuracy. Our analysis extends on the analysis provided by Einkemmer & Ostermann for the semi-Lagrangian method without a rotational grid and builds on the techniques summarized in [10] for the analysis of splitting methods and a Lagrangian-Eulerian viewpoint on the Vlasov equation [7; 11; 14]. Moreover, we will show for the example of ion Bernstein waves that solution of superior quality—in particular with respect to higher modes in both space and time—can be achieved with the rotational grid compared to a pure directional splitting.

The remainder of the article is organized as follows: In the following section, we derive the Vlasov equation in the rotational domain and briefly recapture the semi-Lagrangian method which is applied in the rotating frame. Section 3 considers the temporal splitting method and an analysis of its

convergence properties. Numerical results that verify the error analysis are presented in Section 4 along with the physical test case of nonlinear ion Bernstein waves demonstrating the positive effect of the use of the rotational grid semi-Lagrangian method.

2 Coordinate transformation and semi-Lagrangian discretization

In this section we first transform the Vlasov equation into the rotating frame. Afterwards, we briefly introduce the semi-Lagrangian method which is used to solve the Vlasov equation for a given initial condition.

2.1 Rotating velocity frame

The coordinate transformation of this subsection will remove the $\mathbf{v} \times \mathbf{B}_0$ term in eq. (2) using a rotating velocity grid.

The required moving mesh is based on the coordinate transformation described by Huang & Russell [11, Chap. 3.1]. In order to derive the rotating grid we only need to consider the rotational part of eq. (2)

$$\partial_t f(\mathbf{v}, t) + (\mathbf{v} \times \boldsymbol{\omega}_c) \cdot \nabla_{\mathbf{v}} f(\mathbf{v}, t) = 0 \quad (4)$$

with the cyclotron frequency $\boldsymbol{\omega}_c = q/m\mathbf{B}_0$. Here and in the following we omit the index s for notational simplicity. The distribution function shall now be mapped onto a computational domain Ω_C which rotates with respect to the physical velocity domain Ω . A mapping with the following structure has to be constructed

$$\mathbf{v} = \mathbf{v}(\tilde{\mathbf{v}}, \tau) : \Omega_C \times [0, T] \rightarrow \Omega \quad (5)$$

where $\tilde{\mathbf{v}}$ is the velocity coordinate on the rotating grid and the time of the rotating grid is the same as on the physical grid $t = \tau$. This mapping shall remove the rotational part in eq. (4). First, the derivatives with respect to \mathbf{v} and t are substituted by the derivatives with respect to $\tilde{\mathbf{v}}$ and τ . The gradient operator with respect to $\tilde{\mathbf{v}}$ can be obtained through the chain rule

$$\nabla_{\mathbf{v}} = \sum_i (\nabla_{\tilde{\mathbf{v}}} \tilde{v}_i(\mathbf{v}, t)|_t) \partial_{\tilde{v}_i} = (\mathbf{J}^{-1})^T \nabla_{\tilde{\mathbf{v}}} \quad (6)$$

where \tilde{v}_i is the i -th component of $\tilde{\mathbf{v}}$ and $\mathbf{J}^{-1} = \frac{\partial \tilde{\mathbf{v}}}{\partial \mathbf{v}}$ is the Jacobian of the inverted mapping of eq. (5). Additionally, the partial time derivative with respect to t has to be replaced by a partial derivative with respect to τ and $\tilde{\mathbf{v}}$.

$$\partial_t f|_{\mathbf{v}} = (\partial_\tau f|_{\tilde{\mathbf{v}}})(\partial_t \tau) + \sum_i (\partial_{\tilde{v}_i} f|_\tau)(\partial_t \tilde{v}_i) \quad (7)$$

$$= (\partial_\tau f|_{\tilde{\mathbf{v}}}) + (\nabla_{\tilde{\mathbf{v}}} f|_\tau) \cdot (\partial_t \tilde{\mathbf{v}}) \quad (8)$$

Now we insert eq. (6) and eq. (7) into the rotational part of the Vlasov equation eq. (4)

$$0 = \partial_\tau f(\tilde{\mathbf{v}}, \tau) + (\partial_t \tilde{\mathbf{v}}) \cdot \nabla_{\tilde{\mathbf{v}}} f(\tilde{\mathbf{v}}, \tau) + (\mathbf{v}(\tilde{\mathbf{v}}, \tau) \times \boldsymbol{\omega}_c) \cdot ((\mathbf{J}^{-1})^T \nabla_{\tilde{\mathbf{v}}} f(\tilde{\mathbf{v}}, \tau)) \quad (9)$$

$$= \partial_\tau f(\tilde{\mathbf{v}}, \tau) + (\partial_t \tilde{\mathbf{v}}) \cdot \nabla_{\tilde{\mathbf{v}}} f(\tilde{\mathbf{v}}, \tau) + (\mathbf{J}^{-1}(\mathbf{v}(\tilde{\mathbf{v}}, \tau) \times \boldsymbol{\omega}_c)) \cdot (\nabla_{\tilde{\mathbf{v}}} f(\tilde{\mathbf{v}}, \tau)) \quad (10)$$

The mapping in eq. (5) will remove the rotational part in the Vlasov equation if the following condition is met

$$\partial_t \tilde{\mathbf{v}} = -(\mathbf{J}^{-1}(\mathbf{v}(\tilde{\mathbf{v}}, \tau) \times \boldsymbol{\omega}_c)). \quad (11)$$

If we consider a constant background magnetic field in z -direction $\mathbf{B}_0 = B_0 \hat{e}_z$ We can write the equation as

$$\begin{pmatrix} \partial_t \tilde{v}_x \\ \partial_t \tilde{v}_y \\ \partial_t \tilde{v}_z \end{pmatrix} = \begin{pmatrix} -(\partial_{v_x} \tilde{v}_x) \omega_c v_y + (\partial_{v_y} \tilde{v}_x) \omega_c v_x \\ -(\partial_{v_x} \tilde{v}_y) \omega_c v_y + (\partial_{v_y} \tilde{v}_y) \omega_c v_x \\ -(\partial_{v_x} \tilde{v}_z) \omega_c v_y + (\partial_{v_y} \tilde{v}_z) \omega_c v_x \end{pmatrix} \quad (12)$$

which is satisfied by

$$\tilde{\mathbf{v}} = \mathbf{D}_{\omega_c}(t) \mathbf{v} \quad (13)$$

$$\mathbf{D}_{\omega_c}(t) = \begin{pmatrix} \cos(\omega_c t) & -\sin(\omega_c t) & 0 \\ \sin(\omega_c t) & \cos(\omega_c t) & 0 \\ 0 & 0 & 1 \end{pmatrix}. \quad (14)$$

It can be verified by insertion and defines the mapping between the computational and the physical domain in eq. (5). Solving eq. (4) in on the rotating domain reduces to a trivial problem

$$\partial_\tau f(\tilde{\mathbf{v}}, \tau) = 0. \quad (15)$$

Finally, we map the Vlasov equation in eq. (2) into the computational domain substituting \mathbf{v} by $\tilde{\mathbf{v}}$ and again using eq. (6) which results in

$$\partial_\tau f(\mathbf{x}, \tilde{\mathbf{v}}, \tau) + (\mathbf{D}_{\omega_c}^{-1}(\tau)\tilde{\mathbf{v}}) \cdot \nabla_{\mathbf{x}} f(\mathbf{x}, \tilde{\mathbf{v}}, \tau) + \left(\mathbf{D}_{\omega_c}(\tau) \frac{q}{m} \mathbf{E}(\mathbf{x}, \tau) \right) \cdot \nabla_{\tilde{\mathbf{v}}} f(\mathbf{x}, \tilde{\mathbf{v}}, \tau) = 0. \quad (16)$$

The notation will be simplified in the remainder of the paper. The tilde and τ will no longer be used to highlight the moving velocity mesh. Only if it is essential to distinguish between the physical and the computational domain we will explicitly use $(\tilde{\mathbf{v}}, \tau)$ instead of (\mathbf{v}, t) .

2.2 Solving the Vlasov equation using semi-Lagrangian methods

Before we consider the actual integration methods in the next section we recapture the basic idea of the semi-Lagrangian method which is our chosen numerical method to implement the integrators. A detailed discussion on the semi-Lagrangian method can be found in [9].

The semi-Lagrangian method propagates the distribution function based on the conservation properties of the hyperbolic partial differential equation. The distribution function f is conserved along the trajectories of the so-called characteristic curves. The characteristic curves of the Vlasov equation in eq. (2) are defined by

$$\frac{d}{dt} \begin{pmatrix} \mathbf{X}(t) \\ \mathbf{V}(t) \end{pmatrix} = \begin{pmatrix} \mathbf{V}(t) \\ \frac{q}{m} (\mathbf{E}(\mathbf{X}(t)) + \mathbf{V}(t) \times \mathbf{B}_0) \end{pmatrix}. \quad (17)$$

In the semi-Lagrangian method these characteristics have to be integrated in time using a phase space grid point $(\mathbf{x}_i, \mathbf{v}_j)$ as an initial condition where $\mathbf{i}, \mathbf{j} \in \mathbb{N}^d$ are multi-indexes indicating grid points. We can then use the hyperbolic conservation law to trace the distribution function after a time step h back to an initial condition $f_0(\mathbf{x}, \mathbf{v})$

$$f(\mathbf{x}_i, \mathbf{v}_j, h) = f_0(\mathbf{X}(0; \mathbf{x}_i, \mathbf{v}_j, h), \mathbf{V}(0; \mathbf{x}_i, \mathbf{v}_j, h)), \quad (18)$$

where we denote by $(\mathbf{X}(0; \mathbf{x}_i, \mathbf{v}_j, h), \mathbf{V}(0; \mathbf{x}_i, \mathbf{v}_j, h))$ the solution at time 0 of the characteristic equations starting at $(\mathbf{x}_i, \mathbf{v}_j)$ at time h and solved backwards in time. The point $(\mathbf{X}(0; \mathbf{x}_i, \mathbf{v}_j, h), \mathbf{V}(0; \mathbf{x}_i, \mathbf{v}_j, h))$ is usually not a grid point

of the initial condition. Therefore, the point has to be approximated by numerical interpolation

$$f(\mathbf{x}_i, \mathbf{v}_j, h) = \tag{19}$$

$$I[\{f_0(\mathbf{x}_i, \mathbf{v}_j)\}] \left(\mathbf{x}_i + \int_h^0 \mathbf{V}(t) dt, \mathbf{v}_j + \int_h^0 \frac{q}{m} (\mathbf{E}(\mathbf{X}(t)) + \mathbf{V}(t) \times \mathbf{B}_0) dt \right). \tag{20}$$

Here we denoted by $I[\{f_0(\mathbf{x}_i, \mathbf{v}_j)\}]$ an arbitrary interpolation procedure that defines an interpolant based on the tuples $\{((\mathbf{x}_i, \mathbf{v}_j), f_0(\mathbf{x}_i, \mathbf{v}_j))\}$.

The characteristics of the Vlasov equation in the rotating frame eq. (16) are given by

$$\frac{d}{dt} \begin{pmatrix} \mathbf{X}(t) \\ \mathbf{V}(t) \end{pmatrix} = \begin{pmatrix} \mathbf{D}_{\omega_c}^{-1}(t) \mathbf{V}(t) \\ \frac{q}{m} \mathbf{D}_{\omega_c}(t) \mathbf{E}(\mathbf{X}(t)) \end{pmatrix}. \tag{21}$$

such that the distribution function is advected using

$$f(\mathbf{x}_i, \mathbf{v}_j, h) = I[\{f_0(\mathbf{x}_i, \mathbf{v}_j)\}] \left(\mathbf{x}_i + \int_h^0 \mathbf{D}_{\omega_c}^{-1}(t) \mathbf{V}(t) dt, \mathbf{v}_j + \int_h^0 \frac{q}{m} \mathbf{D}_{\omega_c}(t) \mathbf{E}(\mathbf{X}(t)) dt \right) \tag{22}$$

Since the electric field is dependent of $f(\mathbf{x}, \mathbf{v}, t)$ through the field equations, the advection equation is nonlinear. The numerical analysis of nonlinear equations becomes significantly more difficult. Even if the electric field would be simply a constant background field, we can integrate the characteristic equations but still have to execute an interpolation step in up to six dimensions which is computationally expensive.

It is therefore desirable to reduce the dimensionality of a single advection step to reduce the computational effort and ease the numerical analysis of the advection method. In the next section we use splitting method to split the six dimensional problem in multiple lower dimensional problems which can be solved after one another and are simpler to analyze numerically. The interpolations which we use within this work are briefly described in appendix A.

3 Splitting methods applied to the Vlasov equation

In the previous section we introduced the semi-Lagrangian method and defined the characteristics for the two representations of the Vlasov equation with and without a rotating velocity grid. In this section we utilize splitting methods to decompose the single 6-D advection equation into multiple 1-D advection steps to simplify the solution of the characteristics and the numerical analysis. These are recapitulated in the following section 3.1. In our considerations on splitting methods we assume that the interpolation error is small, and the splitting error is the dominant error of the splitting.

3.1 Splitting methods for differential operators

We briefly recapture the ideas of splitting methods in a generalized abstract concept. For in depth explanations, see Hairer, Lubich & Wanner [10, Sec. II.5, Sec. III.5]. First, consider differential operators of the form

$$D_i = \sum_j A_j^{[i]}(\mathbf{y}) \partial_{y_j} = \mathbf{A}^{[i]}(\mathbf{y}) \cdot \nabla_{\mathbf{y}}, \quad (23)$$

with the phase space variable $\mathbf{y} \in \mathbb{R}^n$. We can build a hyperbolic PDE based on these abstract differential operators

$$(D_1 + D_2)g = 0 \quad (24)$$

where we considered two components. The corresponding characteristics are given by

$$\dot{\mathbf{y}} = \mathbf{A}^{[1]}(\mathbf{y}) + \mathbf{A}^{[2]}(\mathbf{y}) \quad (25)$$

with $\dot{\mathbf{y}}$ being the time derivative of \mathbf{y} . We assume that we can integrate the splitted ordinary differential equations (ODE)

$$\dot{\mathbf{y}} = \mathbf{A}^{[1]}(\mathbf{y}) \quad \dot{\mathbf{y}} = \mathbf{A}^{[2]}(\mathbf{y}) \quad (26)$$

exactly and that the solution of the ODE is described by the flow $\mathbf{y} = \varphi_t^{[i]}(\mathbf{y}_0)$ with $i = 1, 2$.

Then the evolution of any differentiable function $g : \mathbb{R}^n \rightarrow \mathbb{R}$ in eq. (24) can be approximated using exponential integrators. Let us assume the flow

of the characteristics, can be separated into two components, which can be integrated exactly. Then we can advance an initial condition of g in time using D_i with exponential integrators

$$g(\varphi_h^{[i]}(\mathbf{y}_0)) = \left(\sum_{n \geq 0} \frac{h^n}{n!} (D_i^n g) \right) (\varphi_h^{[i]}(\mathbf{y}_0)|_{h=0}) \quad (27)$$

$$= \sum_{n \geq 0} \frac{h^n}{n!} (D_i^n g)(\mathbf{y}_0) = \exp(hD_i)g(\mathbf{y}_0). \quad (28)$$

Here the previously introduced differential operator $D_i g(\mathbf{y}) = \mathbf{A}^{[i]}(\mathbf{y}) \cdot \nabla g(\mathbf{y})$ has been used to substitute the derivative $d^n/dt^n g(\varphi_t^{[i]}(\mathbf{y}_0)) = (D_i^n g)(\varphi_t^{[i]}(\mathbf{y}_0))$.

If we substitute D_i by $D = D_1 + D_2$ in eq. (27), the exponential integrator for eq. (24) is given by

$$g(\varphi_h(\mathbf{y}_0)) = \exp(hD)g(\mathbf{y}_0) = \exp(h(D_1 + D_2))g(\mathbf{y}_0) \quad (29)$$

We can also apply eq. (27) twice to split the integration step into two parts and advect g with both parts separately. Advancing the initial condition y_0 firstly by D_1 and secondly by D_2 we receive

$$g((\varphi_h^{[2]} \circ \varphi_h^{[1]})(\mathbf{y}_0)) = g(\varphi_h^{[2]}(\varphi_h^{[1]}(\mathbf{y}_0))) = \exp(hD_1) \exp(hD_2)g(\mathbf{y}_0), \quad (30)$$

if we utilize eq. (27) recursively. The crucial part to consider here is that if D_1 and D_2 do not commute, such that $[D_1, D_2] \neq 0$, we can not simply merge the two exponential integrators into one which is equal to $\exp(h(D_1 + D_2))$. The relation

$$\exp(hD_2) \exp(hD_1) = \exp(Z(h, D_1, D_2)) \neq \exp(h(D_1 + D_2)) \quad (31)$$

has to be taken into account. Here $Z(h, D_1, D_2)$ is an expansion of terms in powers of h defined through the Baker-Campbell-Hausdorff (BCH) formula. The splitted integrator is exact up to matching orders of the terms in $Z(h, D_1, D_2)$ and the exponent of the right-hand side. The simple integrator defined by eq. (30) is locally of order $O(h^2)$ and called Lie-Splitting. A Strang-Splitting is given by

$$\exp(h/2D_1) \exp(hD_2) \exp(h/2D_1) \quad (32)$$

and is of locally of order $O(h^3)$.

Higher order integrators can be obtained by using m steps instead of two

$$\exp(b_m h D_1) \exp(a_m h D_2) \exp(b_{m-1} h D_1) \dots \exp(a_2 h D_1) \exp(b_1 h D_2) \exp(a_1 h D_1) g(\mathbf{y}_0). \quad (33)$$

The coefficients $a_1, b_1, \dots, a_m, b_m$ have to be determined using eq. (31), such that the terms of the polynomial $Z(h, D_1, D_2)$ vanish up to a given order h^p to obtain an integrator of order p . A detailed explanation on order conditions through the BCH formula is given by Hairer, Lubich & Wanner [10, Sec.III.4,III.5].

If the integration is actually implemented through an algorithm, an appropriate numerical method has to be chosen to actually carry out the integration. This method might introduce further errors based on the time step and errors based on the discretization of space. We use the semi-Lagrangian method section 2.2 to explicitly implement the exponential integrators.

3.2 Splitting propagator for the Vlasov equation in the physical frame

After recapturing the basic ideas of splitting methods we will reduce the 6-D Vlasov equation in eq. (2) down to multiple 1-D advection problems. Additionally, we construct an integrator which is second order accurate, that is each single time step is required to be $O(h^3)$ accurate which is equivalent to a Strang splitting. First we need to identify the differential operators which can be splitted in the Vlasov equation. The \mathbf{x} -advection operator is $\mathbf{v} \cdot \nabla_{\mathbf{x}}$ which defines the transport properties in the spatial domain. The velocity domain transport is defined through the second differential operator $(\mathbf{E}(\mathbf{x}, t) + \mathbf{v} \times \mathbf{B}_0) \cdot \nabla_{\mathbf{v}}$. We split according to these two operators which gives

$$\mathbf{A}_{\mathbf{x}} \cdot \nabla_{\mathbf{x}} = \mathbf{v} \cdot \nabla_{\mathbf{x}} \quad \mathbf{A}_{\mathbf{v}} \cdot \nabla_{\mathbf{v}} = (\mathbf{E}(\mathbf{x}, t) + \mathbf{v} \times \mathbf{B}_0) \cdot \nabla_{\mathbf{v}}. \quad (34)$$

The ODEs defining the splitted flows are then given by

$$\frac{d}{dt} \begin{pmatrix} \mathbf{X}(t) \\ \mathbf{V}(t) \end{pmatrix} = \begin{pmatrix} \mathbf{v} \\ 0 \end{pmatrix} \quad \frac{d}{dt} \begin{pmatrix} \mathbf{X}(t) \\ \mathbf{V}(t) \end{pmatrix} = \begin{pmatrix} 0 \\ (\mathbf{E}(\mathbf{X}(t)) + \mathbf{V} \times \mathbf{B}_0) \end{pmatrix} \quad (35)$$

In our physically interesting examples of section 4.3, a field equation is coupled to the Vlasov equation to determine the electric field. These field equations depend on f only through the particle density n . Therefore, during the

\mathbf{v} advection based on $\mathbf{A}_\mathbf{v}$, f changes only with respect to \mathbf{v} . The particle density n and therefore also the electric field $\mathbf{E}(\mathbf{X}(t))$ do not change such that we can drop the explicit time dependence of the latter in the substep, and we obtain an autonomous ODE defining the flow of f . For autonomous ODE we can utilize the previously introduced framework of exponential integrators to propagate the distribution function in time. A rigorous proof of the second order accuracy of this splitting was provided in Einkemmer & Ostermann[8].

So far we have reduced the six dimensional Vlasov equation into two 3-D problems that can be solved to propagate the Vlasov equation using the vector fields $\mathbf{A}_\mathbf{x}$ and $\mathbf{A}_\mathbf{v}$. Further reduction to multiple 1-D problems is achieved by again splitting the vector fields in the spatial domain A_i with $i = (x, y, z)$ and the velocity domain A_j with $j = (v_x, v_y, v_z)$. A second order integrator based on Strang-Splitting is then given by

$$\begin{aligned}
f(\mathbf{x}, \mathbf{v}, h) + O(h^3) = & \exp\left(\frac{h}{2}A_{v_x}\partial_{v_x}\right) \exp\left(\frac{h}{2}A_{v_y}\partial_{v_y}\right) \exp\left(\frac{h}{2}A_{v_z}\partial_{v_z}\right) \\
& \exp\left(\frac{h}{2}A_x\partial_x\right) \exp\left(\frac{h}{2}A_y\partial_y\right) \exp\left(\frac{h}{2}A_z\partial_z\right) \\
& \exp\left(\frac{h}{2}A_z\partial_z\right) \exp\left(\frac{h}{2}A_y\partial_y\right) \exp\left(\frac{h}{2}A_x\partial_x\right) \\
& \exp\left(\frac{h}{2}A_{v_z}\partial_{v_z}\right) \exp\left(\frac{h}{2}A_{v_y}\partial_{v_y}\right) \exp\left(\frac{h}{2}A_{v_x}\partial_{v_x}\right) f_0(\mathbf{x}, \mathbf{v})
\end{aligned} \tag{36}$$

Since the operators in the spatial domain commute $[A_{x_i}, A_{x_j}] = 0$ we can reduce the computational complexity of the problem by switching and merging operators working on the same axis into a single operation such that we can reduce twelve operations to nine

$$\begin{aligned}
f(\mathbf{x}, \mathbf{v}, h) + O(h^3) = & \exp\left(\frac{h}{2}A_{v_x}\partial_{v_x}\right) \exp\left(\frac{h}{2}A_{v_y}\partial_{v_y}\right) \exp\left(\frac{h}{2}A_{v_z}\partial_{v_z}\right) \\
& \exp(hA_x\partial_x) \exp(hA_y\partial_y) \exp(hA_z\partial_z) \\
& \exp\left(\frac{h}{2}A_{v_z}\partial_{v_z}\right) \exp\left(\frac{h}{2}A_{v_y}\partial_{v_y}\right) \exp\left(\frac{h}{2}A_{v_x}\partial_{v_x}\right) f_0(\mathbf{x}, \mathbf{v})
\end{aligned} \tag{37}$$

This operator gives a convergence rate of order two in the time discretization if other errors sources depending on the time step can be neglected.

The subsection is concluded by combining the splitting with the semi-Lagrangian method of section 2.2. The splitted operators only require to solve a 1-D advection problem with a constant advection coefficient such that the integral solutions of eq. (17) reduce to

$$Y(t_0) = y + \int_{t_0+h}^{t_0} c dt = y - hc \quad (38)$$

with $Y(0) \in (\mathbf{X}(0), \mathbf{V}(0))$ and $y \in (\mathbf{x}_i, \mathbf{v}_j)$. The shifts are explicitly given by.

$$c_x = v_x \quad c_y = v_y \quad c_z = v_z \quad (39)$$

$$c_{v_x} = \frac{q}{m} E_x(\mathbf{x}) + \frac{q}{m} v_y B_0 \quad c_{v_y} = \frac{q}{m} E_y(\mathbf{x}) - \frac{q}{m} v_x B_0 \quad c_{v_z} = \frac{q}{m} E_z(\mathbf{x}) \quad (40)$$

In algorithm 1 all steps are combined to provide the solver for the Vlasov equation. The solver will be compared to the solution on a rotating grid in section 4.3. The subscript of the interpolation indicates the direction of the 1-D interpolation.

Algorithm 1 Solve eq. (2) using operator splitting described in section 3.2 and the semi-Lagrangian method of section 2.2

- 1: Initial condition $f_0(\mathbf{x}, \mathbf{v})$, Time step h , Final time t
 - 2: **while** $t_0 < t$ **do**
 - 3: $f^{[1]}(\mathbf{x}_i, \mathbf{v}_j) = I_{v_x}[\{f_0(\mathbf{x}_i, \mathbf{v}_j)\}](\mathbf{x}_i, \mathbf{v}_j - h/2(c_{v_x}, 0, 0))$
 - 4: $f^{[2]}(\mathbf{x}_i, \mathbf{v}_j) = I_{v_y}[\{f^{[1]}(\mathbf{x}_i, \mathbf{v}_j)\}](\mathbf{x}_i, \mathbf{v}_j - h/2(0, c_{v_y}, 0))$
 - 5: $f^{[3]}(\mathbf{x}_i, \mathbf{v}_j) = I_{v_z}[\{f^{[2]}(\mathbf{x}_i, \mathbf{v}_j)\}](\mathbf{x}_i, \mathbf{v}_j - h/2(0, 0, c_{v_z}))$
 - 6: $f^{[4]}(\mathbf{x}_i, \mathbf{v}_j) = I_x[\{f^{[3]}(\mathbf{x}_i, \mathbf{v}_j)\}](\mathbf{x}_i - h(c_x, 0, 0))$
 - 7: $f^{[5]}(\mathbf{x}_i, \mathbf{v}_j) = I_y[\{f^{[4]}(\mathbf{x}_i, \mathbf{v}_j)\}](\mathbf{x}_i - h(0, c_y, 0))$
 - 8: $f^{[6]}(\mathbf{x}_i, \mathbf{v}_j) = I_z[\{f^{[5]}(\mathbf{x}_i, \mathbf{v}_j)\}](\mathbf{x}_i - h(0, 0, c_z))$
 - 9: $\mathbf{E}(\mathbf{x}_i) = \text{solve electric field}(f^{[6]}(\mathbf{x}_i, \mathbf{v}_j))$
 - 10: $f^{[7]}(\mathbf{x}_i, \mathbf{v}_j) = I_{v_z}[\{f^{[6]}(\mathbf{x}_i, \mathbf{v}_j)\}](\mathbf{x}_i, \mathbf{v}_j - h/2(0, 0, c_{v_z}))$
 - 11: $f^{[8]}(\mathbf{x}_i, \mathbf{v}_j) = I_{v_y}[\{f^{[7]}(\mathbf{x}_i, \mathbf{v}_j)\}](\mathbf{x}_i, \mathbf{v}_j - h/2(0, c_{v_y}, 0))$
 - 12: $f(\mathbf{x}_i, \mathbf{v}_j, t_0) = I_{v_x}[\{f^{[8]}(\mathbf{x}_i, \mathbf{v}_j)\}](\mathbf{x}_i, \mathbf{v}_j - h/2(c_{v_x}, 0, 0))$
 - 13: Set $t_0 = t_0 + h$ and $f_0(\mathbf{x}_i, \mathbf{v}_j) = f(\mathbf{x}_i, \mathbf{v}_j, t_0)$
 - 14: **end while**
 - 15: **return** $f(\mathbf{x}, \mathbf{v}, t)$
-

3.3 Splitting propagator for the Vlasov equation in the rotating frame

In the last subsection the Vlasov equation has been splitted into multiple 1-D problems. This subsection focuses on the Vlasov equation in the rotating frame defined by eq. (16). We can again identify the differential operators in the spatial domain and the velocity domain respectively

$$\mathbf{A}_{\mathbf{x}} = \mathbf{D}_{\omega_c}^{-1}(t)\mathbf{v} \cdot \nabla_{\mathbf{x}} \quad \mathbf{A}_{\mathbf{v}} = \mathbf{D}_{\omega_c}(t)\mathbf{E}(\mathbf{x}, t) \cdot \nabla_{\mathbf{v}}. \quad (41)$$

The ODEs defining the splitted flows are then given by

$$\frac{d}{dt} \begin{pmatrix} \mathbf{X}(t) \\ \mathbf{V}(t) \end{pmatrix} = \begin{pmatrix} \mathbf{D}_{\omega_c}^{-1}(t)\mathbf{V} \\ 0 \end{pmatrix} \quad \frac{d}{dt} \begin{pmatrix} \mathbf{X}(t) \\ \mathbf{V}(t) \end{pmatrix} = \begin{pmatrix} 0 \\ \mathbf{D}_{\omega_c}(t)\mathbf{E}(\mathbf{X}(t)) \end{pmatrix}. \quad (42)$$

We can again follow the arguments of the last subsection to drop the time dependence of the electric field $\mathbf{E}(\mathbf{X}(t))$ due to the constant spatial properties of the distribution function f during the advection step in the velocity domain. The explicit time dependence of the rotation matrices $\mathbf{D}_{\omega_c}(t)$ and $\mathbf{D}_{\omega_c}^{-1}(t)$ can not be removed from the ODEs such that we do not obtain autonomous ODEs to which we could apply the framework of exponential integrators. Fortunately, the rotation matrices are known explicitly and not complex such that order conditions for the flows can be derived by solving the ODEs and calculate the flows explicitly which will be done in the following.

The exact flow that needs to be solved in the rotating frame is given by eq. (21). Advancing the initial condition (\mathbf{x}, \mathbf{v}) by a time step of length h starting from t_0 will be denoted by the mapping

$$\varphi_{t_0+h, t_0} : (\mathbf{x}, \mathbf{v}) \mapsto (\mathbf{X}(t_0 + h), \mathbf{V}(t_0 + h)). \quad (43)$$

The approximated flows defined by the ODEs in eq. (42) are superscripted by the coordinates which are advected by the flow map

$$\varphi_{t_0+h, t_0}^{[\mathbf{x}]} : (\mathbf{x}, \mathbf{v}) \mapsto \left(\mathbf{x} + \int_{t_0}^{t_0+h} \mathbf{D}_{\omega_c}(s)\mathbf{v}ds, \mathbf{v} \right) \quad (44)$$

$$\varphi_{t_0+h, t_0}^{[\mathbf{v}]} : (\mathbf{x}, \mathbf{v}) \mapsto \left(\mathbf{x}, \mathbf{v} + \int_{t_0}^{t_0+h} \mathbf{D}_{\omega_c}(s)\mathbf{E}(\mathbf{x})ds \right). \quad (45)$$

We derive the convergence order of an explicit splitting that approximates the flow map $\varphi_{t_0+h, t_0}(\mathbf{x}, \mathbf{v})$ globally up to second order in time

$$\varphi_{t_0+h, t_0}(\mathbf{x}, \mathbf{v}) = \left(\varphi_{t_0+h, t_0+h/2}^{[\mathbf{v}]} \circ \varphi_{t_0+h, t_0}^{[\mathbf{x}]} \circ \varphi_{t_0+h/2, t_0}^{[\mathbf{v}]} \right) (\mathbf{x}, \mathbf{v}) + R(h). \quad (46)$$

If the residual $R(h)$ only contains components of $O(h^3)$ the splitting has the desired convergence rate. The global convergence order of $O(h^2)$ can then be proved by means of standard arguments of consistency and stability.

We start with the exact expression of the flow and transform it into an expression for eq. (46). Into the exact expression we inserted the approximations $\bar{\mathbf{x}}$ and $\bar{\mathbf{v}}$ to receive a link between the splitted flow map and the exact flow map. The approximation $\bar{\mathbf{x}}$ is the \mathbf{x} component of $(\varphi_{t_0+h,t_0}^{[\mathbf{x}]} \circ \varphi_{t_0+h/2,t_0}^{[\mathbf{v}]}) (\mathbf{x}, \mathbf{v})$. The approximation $\bar{\mathbf{v}}$ is the \mathbf{v} component of $\varphi_{t_0+h/2,t_0}^{[\mathbf{v}]} (\mathbf{x}, \mathbf{v})$. Reorganizing the obtained components provides the splitted flow maps of the

ODEs in eq. (46) as well as the residual $R(h)$.

$$\varphi_{t_0+h,t_0}(\mathbf{x}, \mathbf{v}) = \begin{pmatrix} \mathbf{X}(t_0 + h) \\ \mathbf{V}(t_0 + h) \end{pmatrix} \quad (47)$$

$$= \begin{pmatrix} \mathbf{x} \\ \mathbf{v} \end{pmatrix} + \int_{t_0}^{t_0+h} \begin{pmatrix} \mathbf{D}_{\omega_c}^{-1}(s) \mathbf{V}(s) \\ \mathbf{D}_{\omega_c}(s) \mathbf{E}(\mathbf{X}(s)) \end{pmatrix} ds \quad (48)$$

$$= \begin{pmatrix} \mathbf{x} \\ \mathbf{v} \end{pmatrix} + \int_{t_0}^{t_0+h/2} \begin{pmatrix} 0 \\ \mathbf{D}_{\omega_c}(s) \mathbf{E}(\mathbf{X}(s)) \end{pmatrix} ds \quad (49)$$

$$+ \int_{t_0}^{t_0+h} \begin{pmatrix} \mathbf{D}_{\omega_c}^{-1}(s) \mathbf{V}(s) \\ 0 \end{pmatrix} ds$$

$$+ \int_{t_0+h/2}^{t_0+h} \begin{pmatrix} 0 \\ \mathbf{D}_{\omega_c}(s) \mathbf{E}(\mathbf{X}(s)) \end{pmatrix} ds \quad (50)$$

$$= \begin{pmatrix} \mathbf{x} \\ \mathbf{v} \end{pmatrix} + \int_{t_0}^{t_0+h/2} \begin{pmatrix} 0 \\ \mathbf{D}_{\omega_c}(s) [\mathbf{E}(\mathbf{X}(s)) + (\mathbf{E}(\mathbf{x}) - \mathbf{E}(\mathbf{x}))] \end{pmatrix} ds$$

$$+ \int_{t_0}^{t_0+h} \begin{pmatrix} \mathbf{D}_{\omega_c}^{-1}(s) [\mathbf{V}(s) + (\bar{\mathbf{v}} - \bar{\mathbf{v}})] \\ 0 \end{pmatrix} ds$$

$$+ \int_{t_0+h/2}^{t_0+h} \begin{pmatrix} 0 \\ \mathbf{D}_{\omega_c}(s) [\mathbf{E}(\mathbf{X}(s)) + (\mathbf{E}(\bar{\mathbf{x}}) - \mathbf{E}(\bar{\mathbf{x}}))] \end{pmatrix} ds \quad (51)$$

$$= (\varphi_{t_0+h/2,t_0}^{[\mathbf{v}]} \circ \varphi_{t_0+h,t_0}^{[\mathbf{x}]} \circ \varphi_{t_0+h,t_0+h/2}^{[\mathbf{v}]}) (\mathbf{x}, \mathbf{v}) + R(h). \quad (52)$$

We consider three terms of the residual

$$R(h) = R_1(h) + R_2(h) + R_3(h), \quad (53)$$

which are given by

$$R_1(h) = \int_{t_0}^{t_0+h/2} \begin{pmatrix} 0 \\ \mathbf{D}_{\omega_c}(s) [\mathbf{E}(\mathbf{X}(s)) - \mathbf{E}(\mathbf{x})] \end{pmatrix} ds \quad (54)$$

$$R_2(h) = \int_{t_0}^{t_0+h} \begin{pmatrix} \mathbf{D}_{\omega_c}^{-1}(s) [\mathbf{V}(s) - \bar{\mathbf{v}}] \\ 0 \end{pmatrix} ds \quad (55)$$

$$= \int_{t_0}^{t_0+h} \begin{pmatrix} \mathbf{D}_{\omega_c}^{-1}(s) \left[\mathbf{V}(s) - \left(\mathbf{v} + \int_{t_0}^{t_0+h/2} \mathbf{D}_{\omega_c}(s') \mathbf{E}(\mathbf{x}) ds' \right) \right] \\ 0 \end{pmatrix} ds \quad (56)$$

$$R_3(h) = \int_{t_0+h/2}^{t_0+h} \begin{pmatrix} 0 \\ \mathbf{D}_{\omega_c}(s) [\mathbf{E}(\mathbf{X}(s)) - \mathbf{E}(\bar{\mathbf{x}})] \end{pmatrix} ds, \quad (57)$$

where $\bar{\mathbf{x}} = \mathbf{x} + \int_{t_0}^{t_0+h} \mathbf{D}_{\omega_c}^{-1}(s') \left(\mathbf{v} + \int_{t_0}^{t_0+h/2} \mathbf{D}_{\omega_c}(s'') \mathbf{E}(\mathbf{x}) ds'' \right) ds'$. If the integrals eqs. (54), (56) and (57) only contain terms of order $O(h^3)$ our splitted flow map has the required convergence properties.

We consider only small time steps h such that we can expand the integral solution of eq. (21) and remove higher order terms

$$\mathbf{X}(s) = \mathbf{x} + \int_{t_0}^s \mathbf{D}_{\omega_c}^{-1}(s') \mathbf{V}(s') ds' = \mathbf{x} + \int_{t_0}^s (\mathbf{D}_{\omega_c}^{-1}(s') \mathbf{v} + O(s')) ds' \quad (58)$$

$$\begin{aligned} \mathbf{V}(s) &= \mathbf{v} + \int_{t_0}^s \mathbf{D}_{\omega_c}(s') \mathbf{E}(\mathbf{X}(s')) ds' \quad (59) \\ &= \mathbf{v} + \int_{t_0}^s \left(\mathbf{D}_{\omega_c}(s') \mathbf{E}(\mathbf{x}) + \int_{t_0}^{s'} \mathbf{D}_{\omega_c}^{-1}(s'') \mathbf{v} ds'' \nabla_{\mathbf{x}} \mathbf{E}(\mathbf{x}) + O(s'^2) \right) ds', \quad (60) \end{aligned}$$

where we inserted eq. (21) into the second integral to expand the velocity advection.

Residuals $R_1(h) + R_3(h)$ We first estimate a residual for the $R_1(h) + R_3(h)$. We can insert the integral solution eq. (58) into $R_3(h)$, expand both expressions for the electric field \mathbf{E} with regard to the time shift given by the integral, and keep the terms up to $O(h)$ which is sufficient to show that the

residuum is $O(h^3)$. The intermediate steps are omitted in the following

$$R_3(h) = \int_{t_0+h/2}^{t_0+h} \mathbf{D}_{\omega_c}(s) \left[\mathbf{E} \left(\mathbf{x} + \int_{t_0}^s (\mathbf{D}_{\omega_c}^{-1}(s') \mathbf{v} + O(h)) ds' \right) - \right. \quad (61)$$

$$\left. \mathbf{E} \left(\mathbf{x} + \int_{t_0}^{t_0+h} \mathbf{D}_{\omega_c}^{-1}(s') (\mathbf{v} + \int_{t_0}^{t_0+h/2} \mathbf{D}_{\omega_c}(s'') \mathbf{E}(\mathbf{x}) ds'') ds' \right) \right] ds \quad (62)$$

$$= \int_{t_0+h/2}^{t_0+h} \mathbf{D}_{\omega_c}(s) \left[\left(\int_{t_0}^s \mathbf{D}_{\omega_c}^{-1}(s') ds' - \int_{t_0}^{t_0+h} \mathbf{D}_{\omega_c}^{-1}(s') ds' \right) \nabla_{\mathbf{x}} \mathbf{E}(\mathbf{x}) \right] ds \quad (63)$$

$$+ O(h^3). \quad (64)$$

The residual $R_1(h)$ can be expanded using eq. (58) as well such that it reduces to

$$R_1(h) = \int_{t_0}^{t_0+h/2} \left(\mathbf{D}_{\omega_c}(s) \int_{t_0}^s \mathbf{D}_{\omega_c}^{-1}(s') s' \nabla_{\mathbf{x}} \mathbf{E}(\mathbf{x}) ds' \right) ds + O(h^3). \quad (65)$$

We can sum both residuals and use that the argument of the rotation matrices is $O(h)$ due to the integral boundaries such that we can expand the matrix and integrate only the first non-zero component which is the unity matrix

$$\|R_1(h) + R_3(h)\| \quad (66)$$

$$= \left\| \left(\int_{t_0}^{t_0+h} \int_{t_0}^s \mathbf{D}_{\omega_c}(s-s') ds' ds - \int_{t_0+h/2}^{t_0+h} \int_{t_0}^{t_0+h} \mathbf{D}_{\omega_c}(s-s') ds' ds \right) \nabla_{\mathbf{x}} \mathbf{E}(\mathbf{x}) \right\| \quad (67)$$

$$= \left\| \left(\int_{t_0}^{t_0+h} \int_{t_0}^s (1 + O(h)) ds' ds - \int_{t_0+h/2}^{t_0+h} \int_{t_0}^{t_0+h} (1 + O(h)) ds' ds \right) \nabla_{\mathbf{x}} \mathbf{E}(\mathbf{x}) \right\| \quad (68)$$

$$= O(h^3). \quad (69)$$

Residual $R_2(h)$ The second component of the residual can be considered on its own. We first insert the integral solution for $\mathbf{V}(s)$ given by eq. (60).

Afterwards, we again expand the nonlinearity $\mathbf{E}(\mathbf{X}(s))$ using the integral eq. (58). The remaining integral has the same structure as the final integral of the previous paragraph.

$$R_2(h) \tag{70}$$

$$= \left\| \int_{t_0}^{t_0+h} \mathbf{D}_{\omega_c}^{-1}(s) \left(\int_{t_0}^s \mathbf{D}_{\omega_c}(s') \mathbf{E}(\mathbf{X}(s')) ds' - \int_{t_0}^{t_0+h/2} \mathbf{D}_{\omega_c}(s') ds' \mathbf{E}(\mathbf{x}) \right) ds \right\| \tag{71}$$

$$= \left\| \int_{t_0}^{t_0+h} \mathbf{D}_{\omega_c}^{-1}(s) \left(\int_{t_0}^s \mathbf{D}_{\omega_c}(s') (\mathbf{E}(\mathbf{x}) + O(h)) ds' - \int_{t_0}^{t_0+h/2} \mathbf{D}_{\omega_c}(s') ds' \mathbf{E}(\mathbf{x}) \right) ds \right\| \tag{72}$$

$$= \left\| \int_{t_0}^{t_0+h} \left(\int_{t_0}^s \mathbf{D}_{\omega_c}^{-1}(s-s') ds' - \int_{t_0}^{t_0+h/2} \mathbf{D}_{\omega_c}^{-1}(s-s') ds' \right) ds \mathbf{E}(\mathbf{x}) \right\| + O(h^3) \tag{73}$$

$$= O(h^3). \tag{74}$$

Therefore, we have discussed that all components of $\|R(h)\|$ are of order $O(h^3)$ locally such that we achieve an overall global convergence order of $O(h^2)$.

The subsection is concluded by merging steps within the integrator to reduce the computational effort of a step moving from t_0 to $t_0 + h$. A significant difference to the splitting of the last subsection is that in the rotating frame also the flows, which define the transport properties of the velocity domain, are commuting. This property can reduce the required number of steps within the integrator significantly. If we consider two successive advection

steps the integrator is given by

$$\begin{aligned}
\begin{pmatrix} \mathbf{X}(t_0 + 2h) \\ \mathbf{V}(t_0 + 2h) \end{pmatrix} + O(h^2) = & \left(\varphi_{t_0+2h, t_0+3h/2}^{[v_x]} \circ \varphi_{t_0+2h, t_0+3h/2}^{[v_y]} \circ \varphi_{t_0+2h, t_0+3h/2}^{[v_z]} \circ \right. \\
& \varphi_{t_0+2h, t_0+h}^{[z]} \circ \varphi_{t_0+2h, t_0+h}^{[y]} \circ \varphi_{t_0+2h, t_0+h}^{[x]} \circ \\
& \varphi_{t_0+3h/2, t_0+h/2}^{[v_x]} \circ \varphi_{t_0+3h/2, t_0+h/2}^{[v_y]} \circ \varphi_{t_0+3h/2, t_0+h/2}^{[v_z]} \circ \\
& \varphi_{t_0+h, t_0}^{[z]} \circ \varphi_{t_0+h, t_0}^{[y]} \circ \varphi_{t_0+h, t_0}^{[x]} \circ \\
& \left. \varphi_{t_0+h/2, t_0}^{[v_z]} \circ \varphi_{t_0+h/2, t_0}^{[v_y]} \circ \varphi_{t_0+h/2, t_0}^{[v_x]} \right) (\mathbf{x}, \mathbf{v}). \quad (75)
\end{aligned}$$

The above integrator has merged two half-time steps of $\varphi_{t_0+h, t_0}^{[\mathbf{v}]}$ using two properties. The first property is the commutative property of two flows acting on different axes. The second property is that we can add up to successive flows working on the same axis if the intervals are adjacent to each other, often referred to as "first-same-as-last" property. Merging these steps removes 30% of the required operations during the advection which is an important performance improvement, since advancing the distribution function is the most expensive steps in solving the Vlasov equation. This was discussed in detail in Schild et.al. [18].

Finally, we can reuse algorithm 1 to actually implement a semi-Lagrangian method on a rotating grid. The algorithm does not change. The coefficients remain constant but depend on time which we have to consider while solving eq. (38)

$$X(0) = x - \left(\int_{t_0+h}^{t_0} \mathbf{D}_{\omega_c}^{-1}(t) dt \mathbf{v} \right)_x \quad Y(0) = y - \left(\int_{t_0+h}^{t_0} \mathbf{D}_{\omega_c}^{-1}(t) dt \mathbf{v} \right)_y \quad (76)$$

$$\begin{aligned}
Z(0) &= z - \left(\int_{t_0+h}^{t_0} \mathbf{D}_{\omega_c}^{-1}(t) dt \mathbf{v} \right)_z \\
V_x(0) &= v_x - \left(\int_{t_0+h}^{t_0} \mathbf{D}_{\omega_c}(t) dt \mathbf{E}(\mathbf{x}) \right)_{v_x} \quad V_y(0) = v_y - \left(\int_{t_0+h}^{t_0} \mathbf{D}_{\omega_c}(t) dt \mathbf{E}(\mathbf{x}) \right)_{v_y} \\
& \quad (77)
\end{aligned}$$

$$V_z(0) = v_z - \left(\int_{t_0+h}^{t_0} \mathbf{D}_{\omega_c}(t) dt \mathbf{E}(\mathbf{x}) \right)_{v_z} .$$

4 Numerical comparison of the semi-Lagrangian method with and without a rotating grid

In this section we investigate the behavior of the rotating grid based on different use cases. All simulations have been conducted using the performance portable BSL6D code [4] which is an open source project of the numerical division of the Max-Planck-Institute of Plasma Physics.

4.1 Solving the $\mathbf{v} \times \mathbf{B}_0$ term

We start our investigation solving only the rotational part of the Vlasov equation which is eqs. (4) and (15) and a basic proof of concept. Using $\mathbf{B}_0 = (0, 0, 1)$ we can solve these two equations on a 2-D domain defined by v_x and v_y . The low dimensionality also allows us to fully visualize the distribution function which helps to understand the behavior of the rotating grid. We compare the results of a Strang-Splitting with and without rotating velocity domain with the analytical solution. In the rotating frame we first transform the solution back to the physical domain and afterwards compare against the analytical solution. The transformation from the computational domain into the physical domain based on the inverse mapping of eq. (13).

The initial condition for our test is given by

$$f_0(\mathbf{v}) = \frac{1}{\sqrt{2\pi}} \exp\left(-\frac{(\mathbf{v} - (1, 0, 0))^2}{2}\right), \quad (78)$$

where all occurring physical quantities have been normalized ($q = m = 1$) to one. The solution to the characteristic equations are given by a harmonic oscillator as shown by Chen [5, Subsec. 2.2.1]. We can use the analytical trajectories to solve eqs. (4) and (15) using the semi-Lagrangian method and trace the grid points back to the initial condition. With these trajectories the time dependent distribution function is given by

$$f(\mathbf{v}, t) = f_0(\mathbf{D}_{\omega_c}(t)\mathbf{v}) \quad (79)$$

$$f(\tilde{\mathbf{v}}, t) = f(\mathbf{D}_{\omega_c}^{-1}(t)\tilde{\mathbf{v}}, t) = f_0(\mathbf{D}_{\omega_c}(t)\mathbf{D}_{\omega_c}^{-1}(t)\tilde{\mathbf{v}}) = f_0(\tilde{\mathbf{v}}) \quad (80)$$

where eq. (79) provides the solution in the physical domain while eq. (80) gives the solution in the rotational domain which has been transformed into the physical domain in the first equality.

The solution in the rotating frame is, as expected, a stationary solution. All motion induced by the $\mathbf{v} \times \mathbf{B}_0$ term was removed from the Vlasov equation. A visualization of the rotating state compared to the fixed state is given in fig. 1. The difference of the analytical and the simulation result is given in the L2 norm in fig. 2. We do not plot the error of the rotating grid since the solution only contains unit operations which do not change the initial condition. The error of the Strang-Splitting approach increases linearly over time. The linear increase is superimposed by an oscillating component which has its minima at symmetry position of the initial condition. At $t = (2n-1)\pi$ the solution is mirrored on the v_y axis and at $t = 2n\pi$ the analytical solution is equivalent to the initial condition with $n \in \mathbb{N}$. At these two time steps the oscillatory component of the error of the Strang-Splitting approach is minimal with respect to the analytical solution.

One advantage of the consideration of exactly solvable problems is that these problems provide perfect test cases for unit test in software applications. The described setup of this subsection provides one example of a unit test which continuously monitors the behavior of the BSL6D code[4].

4.2 Solution of the Vlasov equation with constant background fields

In this example we focus on the convergence behavior of the integrators which have been introduced in sections 3.2 and 3.3 for eqs. (2) and (16). We extend the use case of the last subsection to the full Vlasov equation with constant background fields using $\mathbf{E}(\mathbf{x}, t) = \mathbf{E}_0 = (E_0, 0, 0)$ with $E_0 = 0.1$ and adding the advection part in the spatial domain. The electric field is rather small which is consistent with our example in the next subsection. The initial condition for the velocity space is again given by eq. (78). The spatial domain is initialized with a plane wave perturbation

$$f_0(\mathbf{x}) = 1 + \epsilon \sin(k_{0,x}x + k_{0,y}y) \quad (81)$$

using a small perturbation amplitude $\epsilon = 0.1$ and the smallest modes $k_{0,i} = 2\pi/L_i$ with $i = x, y$ which can be represented on the spatial domain. The initial condition is given by the product $f_0(\mathbf{x}, \mathbf{v}) = f_0(\mathbf{x})f_0(\mathbf{v})$.

We can again utilize the semi-Lagrangian method to calculate the analytical solution $f(\mathbf{x}, \mathbf{v}, t)$ by solving the characteristic equations. The trajectories are solved e.g. by Chen [5, Subsec. 2.2.2]. The solution in the rotating frame

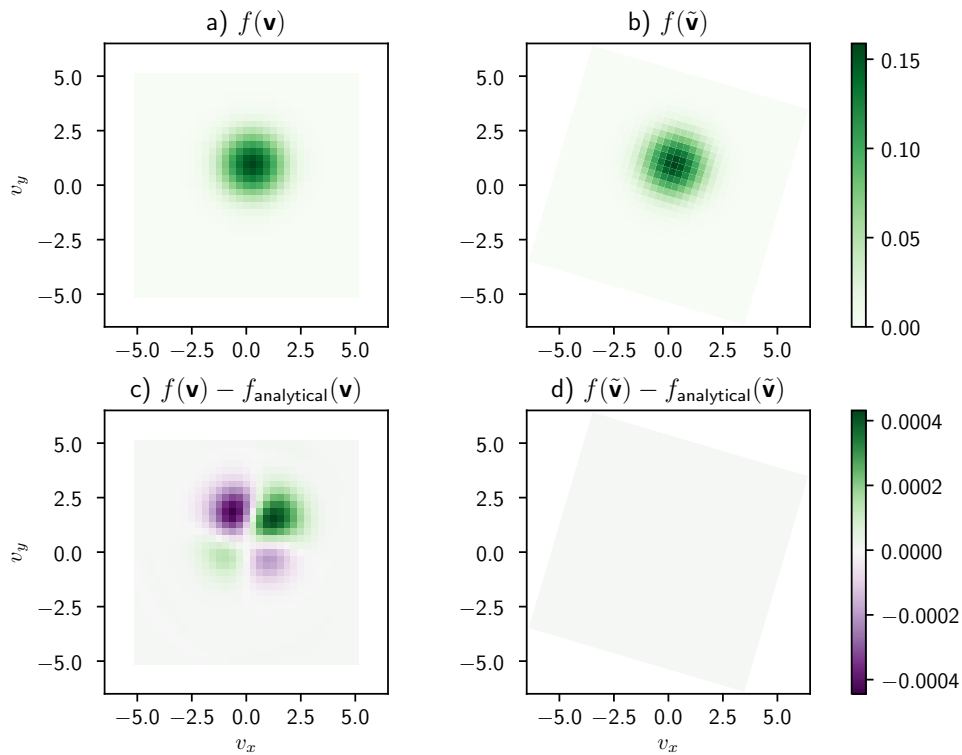


Figure 1: Visualization of the solution of eq. (4) with a classical Strang-Splitting and on a rotating grid in the physical domain at $t = 5/\omega_c$. The figures a) and b) give the full solution while c) and d) show the difference of the simulation results and the analytical solution in eqs. (79) and (80)

is compared by first transforming the initial condition back to the computational domain and afterwards tracing the grid points back to the initial condition. The time dependent distribution function is then given by

$$f(\mathbf{x}, \mathbf{v}, t) = f_0 \left(\mathbf{x} + \int_t^0 \mathbf{D}_{\omega_c}(t') (\mathbf{v} + \mathbf{E}_0) dt' - \mathbf{E}_0 t, \mathbf{D}_{\omega_c}(t) (\mathbf{v} + \mathbf{E}_0) - \mathbf{E}_0 \right) \quad (82)$$

$$\begin{aligned} f(\mathbf{x}, \tilde{\mathbf{v}}, t) &= f(\mathbf{x}, \mathbf{D}_{\omega_c}^{-1}(t) \tilde{\mathbf{v}}, t) \\ &= f_0 \left(\mathbf{x} + \int_t^0 \mathbf{D}_{\omega_c}(t') (\mathbf{D}_{\omega_c}^{-1}(t) \tilde{\mathbf{v}} + \mathbf{E}_0) dt' - \mathbf{E}_0 t, \mathbf{D}_{\omega_c}(t) (\mathbf{D}_{\omega_c}^{-1}(t) \tilde{\mathbf{v}} + \mathbf{E}_0) - \mathbf{E}_0 \right), \end{aligned} \quad (83)$$

where the first result is the solution in the physical domain while the second result gives the solution in the rotational domain which has been transformed into the physical domain in the first equivalence relation.

The difference of the analytical solution and the simulation result is also given fig. 2 using again the L2 norm. The normalization is chosen such that we plot the relative error of the perturbation $\delta f = f - 1$. Now also the error of the solution on the rotating grid increases linearly. But compared to the classical Strang-Splitting approach the error is a magnitude smaller such that we can state that the rotating grid is numerically advantageous compared to a pure Strang-Splitting approach.

Finally, we validate the convergence rates which have been derived in sections 3.2 and 3.3. These simulations have been based on trigonometric interpolation to allow for larger time steps, which would not have been possible with the Lagrange interpolation which does not allow such large time steps in the BSL6D Code[4]. The measured convergence rates are shown in fig. 3. Additionally, to the convergence rates of the Strang-Splitting approaches we added a fourth order splitting schemes which can be constructed based on a Strang-Splitting taken from Kraus et.al. [13, p. 31]

$$\varphi_{h,S4} = \varphi_{\gamma_1 h,S} \circ \varphi_{\gamma_2 h,S} \circ \varphi_{\gamma_1 h,S} \quad (84)$$

with

$$\gamma_1 = \frac{1}{2 - 2^{1/3}} \quad \gamma_2 = -\frac{2^{1/3}}{2 - 2^{1/3}} \quad (85)$$

where $\varphi_{\gamma_i h,S}$ is either the integrator given in section 3.2 or section 3.3. The measured convergence rates match very well the expected convergence rates

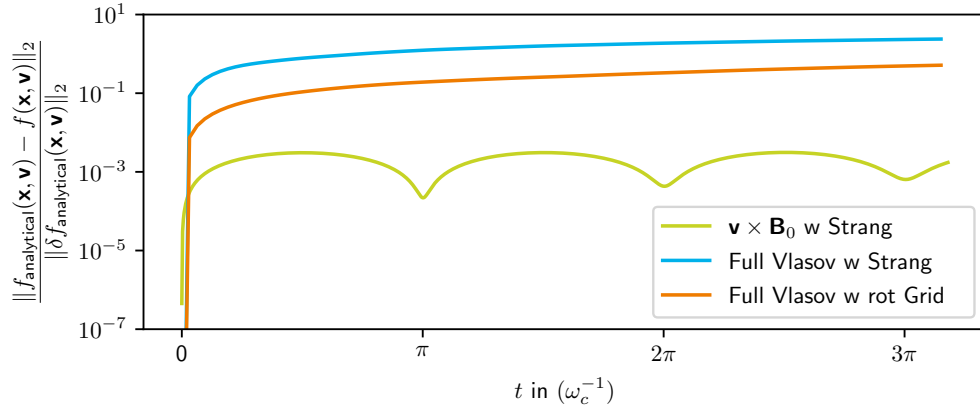


Figure 2: Difference of the analytical solution to simulation results for the test cases in sections 4.1 and 4.2 based on the L2 norm using $h = 0.01/\omega_c$. The error is normalized with respect to the perturbation of the analytical solution $\delta f_{\text{analytical}}$. As is shown in fig. 1 the rotating grid has no numerical error for the $\mathbf{v} \times \mathbf{B}_0$ simulation, which is therefore omitted in the plot.

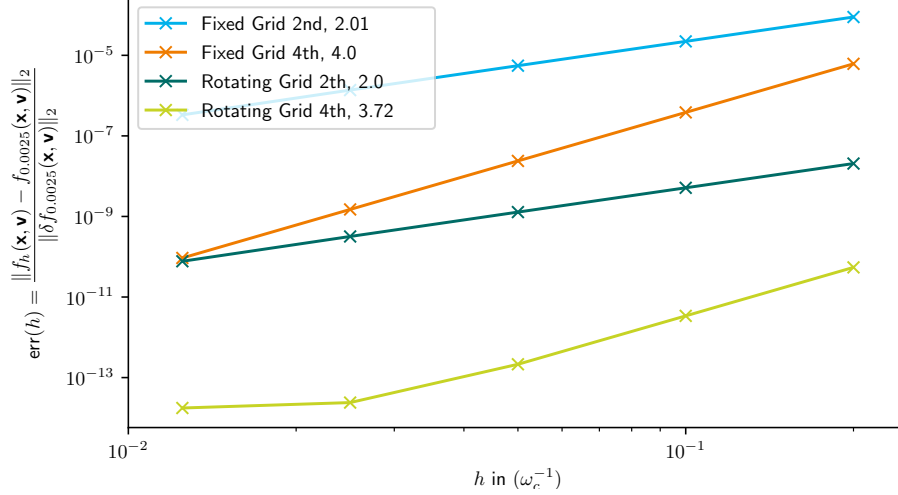


Figure 3: Convergence rates for integrators of sections 3.2, 3.3 and 4.2. The convergence rate in the legend always omit the first data point of the measurement. The errors are estimated against a solution that has been obtained using a significantly smaller time step $h = 0.0025/\omega_c$ and is referred to as a converged solution. The comparison carried out at $t = 9.0/\omega_c$. The difference is normalized on the perturbation δf of the converged solution.

and are calculated using

$$m = \frac{\log(\text{err}(0.2)) - \log(\text{err}(0.025))}{\log(0.2) - \log(0.025)}. \quad (86)$$

Only the fourth order integrator combined with the rotating grid shows deviations from the expected convergence rates for small h . Since the difference between the converged solution and the simulation result is rather small with a difference of 10^{-13} the deviation can be justified by other discretization, rounding, or interpolation errors which dominate in this error regime.

As in the last subsection also this setup provides us with a perfect unit test which is used to continuously validate the behavior of our the implementation in [4].

4.3 Coupling the Vlasov equation to the quasi-neutrality equation

Stable neutralized ion Bernstein waves: Dispersion relation In this last subsection we consider nonlinear examples described by (3). We normalized physical quantities ($e = T = m = 1$) in these equations. The electric field is coupled to the distribution function through the quasi-neutrality condition with adiabatic electrons in eq. (3).

In the first example we reproduce the dispersion relation of neutralizing ion Bernstein waves (nIBW) [3] which have been one central aspects of the study of the limits of gyrokinetics in [15]. The example can be solved as a 3-D problem which consists of the dimensions y, v_x, v_y . The velocity space contains the full rotation and the dispersion relation is reproduced as $\omega(k_y)$. We choose the initial condition to specifically excite nIBWs in the y dimension of our simulation

$$f_0(\mathbf{x}, \mathbf{v}) = f_0(\mathbf{v}) \left[1 + \alpha \sum_{m_{k_y}=1}^{m_{\max}} \sum_{p=0}^{p_{\max}} J_p(k_y v_{\perp}) \cdot \min \left(\frac{1}{e^{-k_y^2} I_p(k_y^2)}, 0.01(p+1)^{1/3} \right) \cdot \operatorname{Re}(e^{iv_{\perp} k_y \sin(\gamma) - p\gamma + k_y y}) \right] \quad (87)$$

Here $I_p(\cdot)$ and $J_p(\cdot)$ are the modified cylindrical Bessel functions and Bessel Functions of the first kind, respectively. Also, the perpendicular velocity $v_{\perp}^2 = v_x^2 + v_y^2$ and the angle $\gamma \triangleleft (v_{\perp}, k_y)$ are needed for the initialization. Finally, α , m_{\max} , and p_{\max} are the perturbation amplitude, the maximal mode and the maximum order of Bessel functions, respectively. The initialization is based on the analytical solution of nIBWs for this numerical example.

After the initialization the simulation is executed to $t = 1000$ using $h = 0.05$. A Fourier transform is applied to the resulting particle density in space and time $n(\mathbf{x}, t)$ to obtain the dispersion relation which is plotted in fig. 4. We can observe a clear quantitative and qualitative difference in our results. The branches of the dispersion relation with a classical Strang splitting are only visible in the range $k_y \in (0, \rho_L^{-1})$ for the first two harmonics of the gyrofrequency ω_c . With the rotating grid we can reproduce the branches of the dispersion relation within the full domain which has been plotted. For higher waves the Lagrange interpolation has damping effects which removes all perturbations of the distribution function. This is not visible in this domain but was shown in [18, p.11-12].

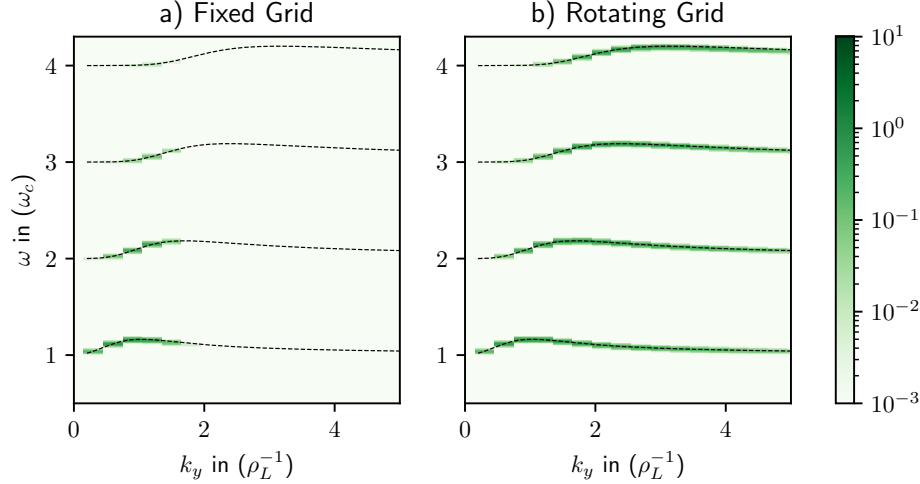


Figure 4: Dispersion relation of neutralizing ion Bernstein waves with a) fixed velocity grid and b) rotating velocity grid. The black dashed lines represent the analytical solution of the example. The length scale is normalized to the Larmor radius ρ_L .

Our conclusion based on this nonlinear numerical example is that the rotating grid is clearly advantageous compared to simple splitting approaches and furthermore allows for a significant reduction of splitting steps due to merging of splitted steps as discussed in section 3.3.

Unstable neutralized ion Bernstein waves: Growth rate The unstable neutralized ion Bernstein waves are also based on eq. (3). But the simulation is executed in a different setup. Neutralized ion Bernstein waves can be destabilized through the imposition of density and temperature gradients [16]. To achieve this, we introduce a right-hand side term to eq. (2), incorporating temperature and density gradients, as outlined in [17]

$$\partial_t f + \mathbf{v} \cdot \nabla_{\mathbf{x}} f + [-\nabla_{\mathbf{x}} \phi + (\mathbf{v} \times \mathbf{B}_0)] \cdot \nabla_{\mathbf{v}} f = \mathbf{v}^* \cdot \nabla_{\mathbf{x}} \phi f_M, \quad (88)$$

where f_M a constant background distribution function $f = f_M + \delta f$ which introduces a density and temperature gradient on the background distribution.

The source on the right-hand side is given by

$$\mathbf{v}^* = \mathbf{B}_0 \times \frac{\nabla n}{n} - \mathbf{B}_0 \times \left(\frac{\nabla T}{T} \frac{3 - (v_x^2 + v_y^2)}{2} \right). \quad (89)$$

Here we use $v_{\perp}^2 = v_x^2 + v_y^2$ which is perpendicular to the magnetic field. The parameters for the gradients are

$$\kappa_n = \frac{\partial_x n}{n} = 0.44; \quad \kappa_T = \frac{\partial_x T}{T} = 0.36. \quad (90)$$

A resolution in configuration space with $N = 1 \times 256 \times 8 \times 33 \times 33 \times 33$ has been chosen for a box with length $L = \pi \times 4\pi \times 80\pi$. The simulation has been performed with a time step of $\Delta t = 0.005$. Figure 5 illustrates a comparison of growth rates between simulations utilizing the rotating grid and the Strang splitting. Additionally, the analytical dispersion relation from [17] for parameter given in (90) is included. Although the simulation with the rotating grid slightly deviates from the analytical results due to numerical damping from spatial advection interpolations, it accurately reproduces the correct growth rate for a significant range of wave numbers. In contrast, in the simulation employing Strang splitting, only the growth rates for the first two wave numbers are accurately reproduced.

5 Acknowledgments

Computations have been performed on the HPC system Raven at the Max Planck Computing and Data Facility. Additionally, we thank Omar Maj and Tileuzhan Mukhamet for fruitful discussions on the convergence analysis and coordinate transformation.

This work has been carried out within the framework of the EUROfusion Consortium, funded by the European Union via the Euratom Research and Training Programme (Grant Agreement No 101052200 — EUROfusion). Views and opinions expressed are however those of the author(s) only and do not necessarily reflect those of the European Union or the European Commission. Neither the European Union nor the European Commission can be held responsible for them.

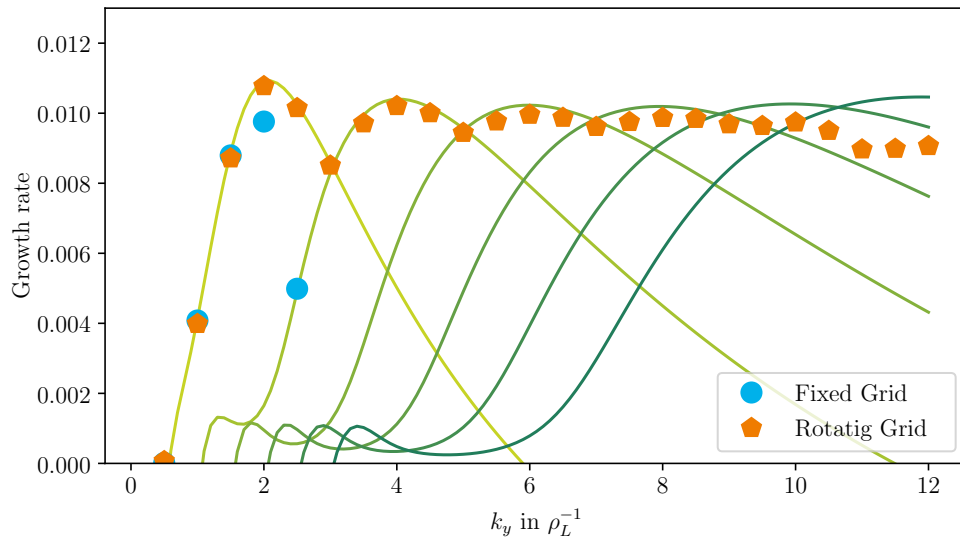


Figure 5: Growth rate of neutralizing ion Bernstein waves with a) fixed velocity grid and Strang splitting and b) rotating velocity grid. The solid lines represent the analytical solution of the growth rates for the first six harmonics of the IBWs with increasing frequency from light to dark green.

A Interpolation Methods

In this paper we use two different interpolations which we briefly introduce. Both assume equidistant grid points $x_j = j\Delta x$, $j = 1, \dots, N$ and interpolate a 1-D function.

The first interpolation is the Lagrange interpolation $L(x)$ which has performance advantages due to its locality as discussed in [18]. The locality has the drawback that the interpolated point has to be centered by the Lagrange interpolation stencil. This can introduce an implementation based CFL condition. Therefore, we assume that the interpolation shift α is smaller than the spacing of the grid Δx . Furthermore, we denote by l_i^q the Lagrange polynomials of order $(q - 1)$ with q nodes in the interpolant

- For an odd number q , the interpolant is given by

$$L(x_j + \alpha) = \sum_{i=j-(q-1)/2}^{j+(q-1)/2} l_i^q(\alpha) f(x_i) \quad (91)$$

- For an even number q , the interpolation stencil is centered around the interpolated point $x_j + \alpha$, such that the interpolation is given by

$$L(x_j + \alpha) = \begin{cases} \sum_{i=j-q/2}^{j+q/2-1} l_i^q(\alpha) f(x_i) \\ \sum_{i=j-q/2+1}^{j+q/2} l_i^q(\alpha) f(x_i) \end{cases} \quad (92)$$

The second interpolation method is a trigonometric interpolation $T(x)$ which is a global formula but more accurate compared to the Lagrange interpolation. The implemented interpolant is given by

- For an even number N of grid points

$$T(x) = \sum_{j=1}^N \frac{\text{sinc}(1/2N((x - x_j)))}{\text{sinc}(1/2(x - x_j))} \cos(1/2(x - x_j)) f(x_j) \quad (93)$$

- For an odd number N of grid points

$$T(x) = \sum_{j=1}^N \frac{\text{sinc}(1/2N((x - x_j)))}{\text{sinc}(1/2(x - x_j))} f(x_j) \quad (94)$$

The trigonometric interpolation could also be based on a Fast Fourier Transform (FFT).

References

- [1] J. BERNIER, F. CASAS, AND N. CROUSEILLES, *Splitting Methods for Rotations: Application to Vlasov Equations*, SIAM J. Sci. Comput., 42 (2020), pp. A666–A697, <https://doi.org/10.1137/19M1273918>.
- [2] N. BESSE AND M. MEHRENBERGER, *Convergence of classes of high-order semi-Lagrangian schemes for the Vlasov–Poisson system*, Math. Comp., 77 (2008), pp. 93–123, <https://doi.org/10.1090/S0025-5718-07-01912-6>.
- [3] M. BRAMBILLA, *Kinetic theory of plasma waves: homogeneous plasmas*, The International series of monographs on physics, Clarendon Press, Oxford ; New York, 1998.
- [4] BSL6D DEVELOPMENT TEAM, *BSL6D*, 2015, <https://gitlab.mpcdf.mpg.de/bsl6d/bsl6d> (accessed 2024/05/02).
- [5] F. F. CHEN, *Introduction to Plasma Physics and Controlled Fusion*, Springer, Cham, 3rd ed. 2016 ed., 2016.
- [6] C. CHENG AND G. KNORR, *The integration of the vlasov equation in configuration space*, Journal of Computational Physics, 22 (1976), pp. 330–351, [https://doi.org/10.1016/0021-9991\(76\)90053-X](https://doi.org/10.1016/0021-9991(76)90053-X).
- [7] J. DONEA, A. HUERTA, J.-P. PONTHOT, AND A. RODRÍGUEZ-FERRAN, *Arbitrary Lagrangian-Eulerian Methods*, John Wiley & Sons, Ltd, Nov. 2004, ch. 14, pp. 413–437, <https://doi.org/10.1002/0470091355.ecm009>.
- [8] L. EINKEMMER AND A. OSTERMANN, *Convergence Analysis of Strang Splitting for Vlasov-Type Equations*, SIAM J. Numer. Anal., 52 (2014), pp. 140–155, <https://doi.org/10.1137/130918599>.
- [9] M. FALCONE AND R. FERRETTI, *Semi-Lagrangian approximation schemes for linear and Hamilton-Jacobi equations*, OT / SIAM, Society of Industrial and Applied Mathematics, SIAM, Philadelphia, Pa, 2014.

- [10] E. HAIRER, C. LUBICH, AND G. WANNER, *Geometric numerical integration: structure-preserving algorithms for ordinary differential equations*, Springer series in computational mathematics, Springer, Berlin ; New York, 2nd ed ed., 2006.
- [11] W. HUANG AND R. D. RUSSELL, *Adaptive moving mesh methods*, Applied mathematical sciences (Springer-Verlag New York Inc.), Springer, New York, NY, 2011.
- [12] K. KORMANN, K. REUTER, AND M. RAMPP, *A massively parallel semi-Lagrangian solver for the six-dimensional Vlasov–Poisson equation*, The International Journal of High Performance Computing Applications, 33 (2019), pp. 924–947, <https://doi.org/10.1177/1094342019834644>.
- [13] M. KRAUS, K. KORMANN, P. J. MORRISON, AND E. SONNENDRÜCKER, *GEMPIC: geometric electromagnetic particle-in-cell methods*, J. Plasma Phys., 83 (2017), pp. 905830401–905830451, <https://doi.org/10.1017/S002237781700040X>.
- [14] T. MUKHAMET, *An arbitrary Lagrangian Eulerian discontinuous galerkin method for Vlasov equation with a strong magnetic field*, 2023.
- [15] M. RAETH, *Beyond gyrokinetic theory: Excitation of high-frequency turbulence in 6d Vlasov simulations of magnetized plasmas with steep temperature and density gradients*, 2023, https://mediatum.ub.tum.de/node?id=1703830&change_language=en.
- [16] M. RAETH AND K. HALLATSCHEK, *High frequency non-gyrokinetic turbulence at tokamak edge parameters*, Phys. Rev. Lett., (2023), <https://doi.org/10.48550/arXiv.2310.15981>.
- [17] M. RAETH, K. HALLATSCHEK, AND K. KORMANN, *Simulation of ion temperature gradient driven modes with 6D kinetic Vlasov code*, Physics of Plasmas, 31 (2024), p. 042101, <https://doi.org/10.1063/5.0197970>.
- [18] N. SCHILD, M. RÄTH, S. EIBL, K. HALLATSCHEK, AND K. KORMANN, *A performance portable implementation of the semi-Lagrangian algorithm in six dimensions*, Computer Physics Communications, 295 (2024), p. 108973, <https://doi.org/10.1016/j.cpc.2023.108973>.

- [19] H. SCHMITZ AND R. GRAUER, *Comparison of time splitting and backsubstitution methods for integrating Vlasov's equation with magnetic fields*, Computer Physics Communications, 175 (2006), pp. 86–92, <https://doi.org/10.1016/j.cpc.2006.02.007>.